Modelling snowfall in southern Italy: a historical perspective in the Benevento Valley (1645-2018)

Nazzareno Diodato, Iñigo Gómara, Gianni Bellocchi

Modelling snowfall in southern Italy: A historical perspective in the Benevento Valley (1645-2018)

Nazzareno Diodato[1], Iñigo Gómara[2,3]* and Gianni Bellocchi[1,4]

[1]*Met European Research Observatory - International Affiliates' Program of the University Corporation for Atmospheric Research, Benevento, Italy;* [*https://orcid.org/0000-0003-3607-8523*](https://orcid.org/0000-0003-3607-8523)

[2]*Departamento de Física de la Tierra y Astrofísica, Universidad Complutense de Madrid, 28040 Madrid, Spain;* [*https://orcid.org/0000-0001-8721-0307*](https://orcid.org/0000-0001-8721-0307)

[3]*Instituto de Geociencias (IGEO), UCM-CSIC, 28040 Madrid, Spain*

[4]*Université Clermont Auvergne, INRAE, VetAgro Sup, UREP, Clermont-Ferrand, France;* [*https://orcid.org/0000-0003-2712-7979*](https://orcid.org/0000-0003-2712-7979)

*Corresponding author: Dr. Iñigo Gómara, Universidad Complutense de Madrid, 28040 Madrid, Spain. E-mail: i.gomara@ucm.es

ABSTRACT

The lack of long-term, homogeneous snowfall records is a limitation in environmental studies. Statistical modelling holds potential to extend back in time snowfall records with a limited set of predictors: snow severity and winter-spring temperatures (with their variability) to reflect elevation influences. The annual number of snow days (SDY) in the Benevento Valley (southern Italy) was detailed for the period 1870-2018. Calibrated in the period 1870–1968 (R^2=0.85) and validated in the period 1969-2018 (R^2=0.67), the model developed here enabled the reconstruction of a time-series of SDY between 1645 and 2018. This unique series (the longest in southern Italy) shows that SDY peaked during the Little Ice Age (until ~1850), dominated by cold air masses or characterized by winter seasons extending until May (1655, 1684, 1763 and 1830) or June (1620). After the change-point detected in 1866, the modelled SDY time-series declined rapidly (Modern Warming Period, 1867-2018). The atmospheric conditions that favoured snowfall in the Benevento Valley throughout the study period were generally associated with an anomalous high-pressure system located over northern-north-western Europe and a low in the eastern Mediterranean. This configuration allowed the incursion of cold continental air from the east-northeast into southern Italy. Our results are consistent with similar studies of snowfall in other European and mid-latitude regions of the northern hemisphere.

Running page head: Longest snowfall reconstruction in southern Italy.

Key words: Climate Variability and Change, Historical reconstruction, Modelling, Snowfall, Southern Italy.

1. INTRODUCTION

In hydrological studies, spatial and temporal heterogeneity is a main challenge for observing, understanding and modelling snowfall, snow accumulation and snowmelt, which are among the processes that have the greatest impact on the global water cycle (Webster et al. 2018). Snowfall occurrence in the northern Hemisphere indicates that winter periods in western Europe (including Italy) are characterized by only a few days of snow per year (Jennings et al. 2018). Different aspects of extreme climate (e.g., extreme cold and snow) are of interest in understanding regional climate characteristics because their changes have impacts for water resources, ecosystems and society, with far-reaching environmental and socio-economic implications (Braconnot & Vimeux 2020).

To support global water-cycle modelling, the number of snow days per year (days with snow depth equal or greater than 1 cm) is an important climatological indicator (WMO 2009) of winter-snow storage, especially in areas where snow falls infrequently. Snowfall delays the transfer of precipitation to surface runoff, infiltration and streamflow generation. In this way, it affects the timing and magnitude of peak flows (Wang et al. 2017), the recession of hydrographs (Yarnell et al. 2010), the onset of snowmelt-driven streamflow (Grundstein & Mote 2010), and the magnitude and duration of summer baseflow (Godsey et al. 2014). However, defining these impacts is difficult and they have only been explored on a large scale. For instance, the variability of autumn snowpack in Eurasia can drive the atmospheric circulation in the northern Hemisphere (Henderson et al. 2018).

Ongoing snow measuring networks are not yet well established at regional and local scales, especially in remote regions (DeWalle & Rango 2008). In the absence of continuous and reliable data, consultation of historical press reports can help to extend and improve the time-series of snowfall events, but characterisation of the temporal and spatial distribution of the snowfall and the associated synoptic patterns remains limited to a few decades (Martínez-Ibarra et al. 2019). Regional investigations using satellite data focus mainly on the extent of snow cover on a global and continental scale, and only refer to the last few decades, during which several satellite missions have been launched or planned (Capozzi et al. 2020). Thus, the understanding of snowfall patterns in several world regions remains limited due to the brevity of the record and poor knowledge of the hydroclimatic mechanisms that control snowfall dynamics.

In Europe, the occurrence of snowfall and the number of snowy days are mainly dependent on latitude and the large-scale atmospheric circulation (Croce et al. 2018), even if snowfall frequency and intensity do not show clear spatial patterns (Navarro-Serrano & López-Moreno 2017). In Italy, snow is common in all mountains, occasionally falling at low elevations and not unfrequently in the northern plains, along the Adriatic coast (east side) and in hinterland areas of the central and southern regions. However, during the centuries of the Little Ice Age (LIA, ~1300-1850 CE; Miller et al. 2012), snowfall was more abundant throughout Italy. During the LIA, the climate was highly variable in Europe, and winters were characterized by very cold and snowy weather. This period coincides with an increase in atmospheric radiocarbon (Stuiver & Braziunas 1993), several intense volcanic eruptions (Briffa et al. 1998) and a decrease in solar activity with a low sunspot number (Lean et al. 1995). The snow-capped volcano Vesuvius (1281 m a.s.l.), depicted in the 19th century anonymous painting in Fig. 1, shows that in the past there were cold snaps and severe snowfall also in places, such as southern Italy, where the climate is generally mild and temperate today.

Studies aimed at collecting, reconstructing and analysing snowfall episodes began in Italy in 1681 with the publication of *La Figura della neve* ("The shape of snow") by the Italian natural philosopher and Catholic priest Donato Rossetti (1633-1686), who described the configuration of snow crystals seen through a microscope. Italy is home of the longest series of daily snow records in the world, starting in Rome in 1741 (Mangianti & Beltrano 1991) and in Turin in 1788 (Mercalli & Di Napoli 2008). Enzi et al. (2014) provided a historical perspective of snowfall occurrence in Italy back to the LIA. More recent studies showed that distinct climatic patterns played an important role in driving snowfall fluctuations over centennial time-scales (Diodato et al. 2019), and that temperature and precipitation changes are dominant controlling factors of hydrological changes (Diodato & Bellocchi 2020). However, no specific assessment of long-term snowfall dynamics in southern Italy (below the 42nd parallel) was reported in previous studies.

Here, we present an annually resolved reconstruction of snow days per year (SDY) in the period 1645-2018 for the Benevento Valley (BNV). Extending southwest of Benevento (41° 08' N, 14° 47' E), the BNV hosts the longest time-series of observed snowfall in southern Italy. Benevento city observatory (BNOBS) and the Met European Research Observatory (MetEROBS), 5-km apart within the BNV, offer a unique heritage of snowfall data to understand and interpret the snowfall regime of the prevalently Mediterranean climate that characterizes this inland valley. This was done with a physically consistent statistical model, hereafter referred to as NLMRM (Non-Linear Multivariate Regression Model). First, we developed a parsimonious model for the reconstruction of the SDY data from climate anomalies related to snowfall severity, mean winter and spring air temperatures, and their standard deviations (Section 2). Then, we used the model to capture climate variability at multiple timescales and to identify patterns of change in snowfall in the BNV over the period 1645 to 2018 and sub-periods (Section 3). We discussed the analysis of historical snowfall in the BNV (Section 4) and concluded the article with a summary of results and future research directions (Section 5).

2. MATERIALS AND METHODS

2.1 Environmental setting

The southern peninsular part of Italy stretches from the area south of Rome (below 42° N) to the most southerly provinces of Apulia (around the 40th parallel) and Calabria (around the 38th parallel). The Benevento Valley is located in the Campania Region, within the southern Apennine range (Figs. 2A,B). Centred around 41° 11' N and 14° 27' E, and with elevations ranging from over about 100 to about 300 m a.s.l., the BNV has an area of about 100 km^2 (Fig. 2C) at the transition between the central and southern Apennines. The Benevento Valley has a typical hot summer Mediterranean climate (Köppen Csa) with more continental features than the maritime (sub-tropical) climate of the Tyrrhenian coast (e.g., around the volcano Vesuvius). According to De Renzi (1829), *The western and southern winds have little influence over this province, less so than the mountains that surround it... The winds of the north-east, and of the north-west, are those which blow there with the greatest impetus. ... But there are places where the west and south winds blow furiously, after crossing the gorges of the mountains, where they have gained strength*.

Synoptic large-scale configurations favourable for snowfall and snow persistence in the BNV are generally associated with the negative phases of the North Atlantic Oscillation (NAO), a see-saw pattern of mean sea-level pressure between the sub-polar and sub-tropical latitudes of the North Atlantic (Pinto & Raible 2012). Under a negative NAO phase (NAO-), a meandering and relatively weak extratropical jet stream favours the incursion of cold Siberian or Arctic air over central and southern Europe. For the former to occur, a low-pressure system is typically located over southern Italy, associated with an anticyclone over Scandinavia (Fazzini et al. 2005). For the incursion of Arctic air, the anticyclone must be located further upstream in the North Atlantic, favouring the advection of air from the north instead of the north-east (D'Errico et al. 2020). Another recurrent configuration is the placement of a low-pressure system south of Italy (over the Ionian Sea) and an anticyclone over northwest Europe (Dafis et al. 2016), bringing over the BNV cold air from the Balkan Peninsula that moistens after crossing the Adriatic Sea. Local orographic features also favour occasional snowfall and snow cover in the BNV, as cold air can be trapped in the area due to vertical thermal inversion. Seasonal and monthly patterns in the BNV (Fig. 3) indicate that snow falls mainly from December to March (rarely in November and April). While mean snow depths in the winter months are rather contained to a few millimetres, the monthly 90th percentiles are expected to be over 40 cm.

2.2 Observatories and data resources

Weather data in the BNV were mostly derived from the observatories of Benevento (BNOBS) and Monte Pino (MetEROBS), at 180 and 170 m a.s.l., respectively (Fig. 2C). We refer here to the BNV homogenized time-series of observed SDY, covering the period from the winter 1869-1870 to 2017-2018 (Diodato & Bellocchi 2020). This time-series was created from the BNOBS and MetEROBS data, and additional data from the former *Servizio Idrografico e Mareografico Nazionale* (Italian Hydrographic and Tidal Service;

SIMN, 1991-1997) observatory, which was about 400-m away from the BNOBS. The latter started its records in 1870, under the guidance of Nicola Orazio Albino, and stopped them in 1968. The SDY series at MetEROBS is continuous from its start in 1985 until today (Diodato 1997). Before 1985, the BNV time-series of observed SDY data is divided into five main periods: (i) 1870-1886, including the observations made by Ambrogio Di Renzo; (ii) 1887-1910, with the observations of Venanzio Vari; (iii) 1911-1949, reconstructed by Diodato and Bellocchi (2020); (iv) 1950-1968, with the measurements of Nazario Doretti; and (v) 1969-1984, which embraces the observations of the former SIMN. SIMN snow observations before 1969 are available with discontinuities and were not used. The SIMN time-series (1969-1984) is the one that presents a relative lower reliability than BNOBS and MetEROBS because the station was not always manned, and snow collection did not systematically take place. BNOBS and MetEROBS were monitored 24 hours a day and the snowfall data were validated at the observation time. The BNOBS series would have been the longest if some data had not been lost during the World War II, when regular measurements stopped until 1949 (Doretti 1950). For the period of missing data (1911-1949), we relied on the data modelled by Diodato and Bellocchi (2020) based on SDY data from neighbouring sites. The SDY observations of the most recent period (1985-2018) have been taken directly by the authors at MetEROBS, which is the only operational weather observatory delivering continuous snow measurements since 1985 in the BNV. In fact, the operational monitoring networks of the *Centro Funzionale Multirischi Protezione Civile della Regione Campania* (Multirisk Functional Centre of Civil Protection–Campania Region; http://centrofunzionale.regione.campania.it/#/pages/dashboard), which has replaced the SIMN, were not set up to perform snow observations. The Mann-Whitney-

Pettitt test (Pettitt 1979), widely used to assess the homogeneity of the distribution of hydro-meteorological variables (Xie et al. 2014), did not detect any abrupt changes ($p > 0.05$) in the distribution of the homogenized SDY data. This supports our assumption that limited changes in geographic location and elevation (and observer changes) do not critically bias the unique realization of the joint time-series (with no overlapping periods for observation site data).

2.3 Gridded climatic datasets

The following gridded climatic datasets were used in this study:

- **The European seasonal reconstruction of air temperatures:** Temperature data for the period 1645-2002, with a horizontal resolution of 0.5° (Luterbacher et al. 2004), were considered to reconstruct SDY back to 1645 (interpolated to the nearest BNV grid-point). We used seasonal winter (December to February) and spring (March to May) temperatures. For the exceptionally cold conditions of 1684 (with an expected return period of ~1000 years), we used the seasonally adjusted mean temperatures derived by Diodato and Bellocchi (2011) for southern Italy, i.e., 0.1 and 7 °C for winter and spring respectively (instead of 4.1 and 11 °C from the regional reconstruction). Once the SDY time-series was reconstructed, its trends and variability where also analysed based on this gridded dataset (Section 3.3).
- **The European monthly reconstruction of mean sea-level pressure (mslp):** The available period 1659-1999 of surface pressure reduced to mean sea-level data (hPa) at 5° horizontal resolution (Luterbacher et al. 2002) was considered to analyse trends and variability of SDY.

- **The Climatic Research Unit (CRU) time-series of variations in climate with variations in other phenomena v3:** Both seasonal temperature (°C) and mslp (hPa) abovementioned reconstruction datasets (Jones & Harris 2008) were updated from the Climatic Research Unit (CRU) global climate data until 2018.
- **The Last Millennium Reanalysis (LMR) Project, Global Climate Reconstructions Version 2*:*** Sea-surface temperatures (°C) at 2° horizontal resolution were retrieved globally as annual ensemble means to evaluate SDY trends and variability. The period considered was 1645-2000 (Tardif et al. 2019).
- **The sea-surface temperature (SST) and sea ice data from the Met Office Hadley Centre (HadISST):** The global monthly 1° sea-surface temperature (°C) dataset from 1870 onwards (Rayner et al. 2003) was also analysed for the period 1870-2018 to evaluate SDY trends and variability.

2.4 Climate indices

The following climate indices were considered in this study:

- **Snow-Severity Index:** As a covariate for SDY modelling, we referred to the snow-severity index (SSI) developed by Diodato et al. (2019). It establishes five classes of snow severity, discernible in narrative texts drawn from historical documentation, from SSI = 0, which identifies winters without comments on their severity or their impacts on the society and economy to SSI = 4, which records extraordinarily snowy winter seasons with a low recurrence rate over many years.
- **The Pacific Decadal Oscillation (PDO) index:** The PDO is a recurring sea surface temperature (SST) anomaly pattern in the North Pacific with ~40-yr periodicity (warm/cold phases) and reported global impacts in climate and marine ecosystems

(Mantua & Hare 2002). The PDO index available from the LMR reanalysis (1645-2000; Tardif et al. 2019) was utilized to assess SDY variability.

- **The Atlantic Multidecadal Oscillation (AMO) index:** The AMO refers to a warming/cooling pattern of multidecadal North Atlantic SST anomalies with ~60-yr periodicity (Knight et al. 2006). The AMO index also available from LMR (1645-2000) was considered for SDY variability analysis.
- **The North Atlantic Oscillation (NAO) index:** As described in the introduction, the NAO is a see-saw pattern of mean sea-level pressure that characterises the strength and location of the westerly flow in the North Atlantic. Additional to the NAO index available from LMR (1645-2000), the winter NAO index reconstruction from Trouet et al. (2009) for the period 1645-1995 and the NAO Gibraltar-Stykkisholmur index (1821-2000) from Jones et al. (1997) were also considered for comparison on SDY variability assessment.

2.5 Development and assessment of the statistical model

In order to minimize uncertainties arising from SDY data estimation, we developed a non-linear multivariate regression model with three predictors and five parameters. Following the principle of parsimony (Mulligan & Wainwright 2013), for which parsimonious modelling has greater explanatory prediction power and lower complexity, we constructed a parsimonious model that could be easily parameterized and validated. The model was sufficiently reliable to be used to reconstruct long-term historical SDY. To increase skill prediction and reduce uncertainties in the modelling estimation of annually resolved SDY data, we performed a multivariate nonlinear regression with four input variables and five parameters considering the original observational period 1870-2018.

This original SDY data (149 years) was segregated into two groups: about two-thirds (99 years) were used for calibration (1870-1968) and the rest (50 years) for validation (1969-2018). In this way, the calibration work was brought into line with the reality of past snowfall to allow a reasonably accurate reconstruction of historical snow days. As a first step, to minimize the number of inputs, we evaluated the effect of individual variables, or groups of variables, on SDY during climatically inhomogeneous but effective periods to take into account different situations. An iterative process (trial-and-error to compose the relevant drivers) subsequently allowed us to explain the dynamics of SDY in relatively simple way. A multi-stage selection logic was used to alternate between term addition and deletion and derive the following non-linear multivariate regression model to estimate SDY (d yr^{-1}) at BNV:

$$\mathrm{SDY(BNV)} = \mathrm{A} \cdot [(\varphi + \mathrm{SSI})^{\eta} + (\beta - \mathrm{Tw} - \mathrm{Ts})^{\sigma} \cdot \mathrm{VC}(\mathrm{Tw} \rightarrow \mathrm{s})_{t=-1}^{t=0}] \qquad (1)$$

where: A (d yr^{-1}) is a scaling parameter relative to the number of SDY when the term in brackets is equal to one, φ and β (°C) are position parameters; η and σ are shape parameters. The first term of Eq. (1) includes the snow-severity index (SSI), which contains a qualitative information relating snowfall anomalies at local scale. In addition to this qualitative term, winter (*Tw*) and spring (*Ts*) temperatures indicate that changes in SDY are temperature-driven, mostly associated with long-distance transport of warm or cold air masses over the European continent. In fact, a rise in temperature will lead to more precipitation in the form of rain and more snowmelt (Croce et al. 2018). The last term in Eq. (1) represents the temperature variability, expressed as the coefficient of variation (*VC*) calculated as the ratio between the standard deviation and the mean of the temperature values from December to May (including winter and spring temperatures, *Tw* and *Ts*, of the previous and current year, t=-1 and t=0). This term is a key factor in inferring seasonal temperature fluctuations, as it is higher in the presence of snow (Diodato et al. 2020a).

The BNV, situated at a mean latitudinal position of Italy and surrounded by mountains, experiences a wide range of climatic characteristics common to those occurring in most of peninsular Italy (Diodato & Bellocchi 2020). The concept of the model (Fig. 4) summarizes the mechanisms mainly driving the common patterns of change of snow-cover extent and duration, and of snow days. It shows that in Italy, ~10-15 % of the territory (central tendency) is covered by snow over winter. In this season, percentiles above the 50th percentile of the fraction of snow-cover extent deviate more from the central values than in other seasons. This indicates that SSI > 0, which captures extreme snowfall years (roughly above the median), is an important driver of snowfall, as it reflects the winter snowfall regime. Snowfall then responds to local temperature forcing during the winter and spring months. In contrast to the Italian mountain chains, where the increase in snow depth is mainly controlled by winter precipitation, temperature control is dominant in transient snow regions (Clark et al. 1999).

The parameters from Eq. (1) were calibrated with the SDY observed at BNV according to the criteria below:

$$\begin{cases} \mathrm{R}^2 = \max \\ \mathrm{MAE} = \min \\ |b-1| = \min \end{cases} \tag{2}$$

The first condition maximizes the determination coefficient ($0 \leq R^2 \leq 1$, optimum), i.e., the variance explained by the model. The second condition minimizes the distance between modelled versus observed SDY data, reducing the mean absolute error (optimum, $0 \leq$ MAE $< \infty$), in d yr^{-1}. The last condition approximates the unit slope of the straight line of the linear regression of the actual versus modelled data (b = 1, optimum). In addition, the Kling-Gupta index ($-\infty <$ KGE ≤ 1) was considered as a measure of efficiency (Kling et al. 2012), where KGE > –0.41 indicates that a model performs better than the mean of the observations as a benchmark predictor. To select the set of relevant covariates for the parsimonious modelling of SDY, we iteratively added in predictors (one at a time) until small MAE and large R^2 values were obtained. The third criterion then determined the final selection. Convergence was obtained by repositioning each predictor in > 50 iterations. Analysis of variance (ANOVA) was then performed to find out whether predictors were all necessary (and not redundant) for the modelling approach. The Durbin-Watson (DW) test was used to assess autocorrelation in model residuals.

Modelling construction and evaluation was carried out in this work with the statistical and graphic software STATGRAPHICS (https://www.statgraphics.com) and WESSA (http://www.wessa.net). Exploratory and time-series analyses (breakpoint detection tests, wavelet power spectrum) were performed using AnClim (http://www.climahom.eu/software-solution/anclim), PAST routines (https://palaeo-electronica.org/2001_1/past/issue1_01.htm) and MATLAB functions (https://www.mathworks.com/products/matlab.html).

3. RESULTS

3.1 Model parameterization and evaluation

With the calibrated parameters of Eq. (1) – $A = 20$, $\varphi = 0.25$, $\eta = 1.4$, $\beta = 28.5$ °C and $\sigma = 2$ – the model approximated the actual data. Fig. 5A shows a satisfactory agreement between observations and estimates, as the points tend to line up around the 1:1 line, with only one outlier (year 1906, black square in the scatterplot, with 5.5 modelled snowy days against one observed) in the 99-year dataset (~1%), which was not considered for model calibration. The R^2-value indicates that the NLMRM SDY(BNV) explains 85% of the variance in actual data. The regression line has a y-intercept a = -0.36 ± 0.34 and slope b = 1.08 ± 0.07 near the optimum values (a = 0 and b = 1). Although a few zero-values on the x-axis indicate that the predictive ability of the model is lower for SDY values close to zero, the intercept is not statistically different from zero (Student-t $p > 0.05$). The MAE, equal to 1.02 d yr^{-1}, depicts a lower value than the standard error of the residuals (1.29 d yr^{-1}), while the Kling-Gupta index is 0.54. There is no indication of serial autocorrelation in the residuals (DW = 1.78, $p > 0.05$). The model residuals return a normal distribution shape (Fig. 5B; Jarque-Bera test $p > 0.05$) and the quantile-quantile (Q-Q) plot (Fig. 5C) shows a distribution of sample-quantiles around the theoretical line, indicating only a few skewed high SDY values.

In the validation phase, R^2 (with a = -0.50 ± 0.49 and b = 1.12 ± 0.16) indicates that the model explains 67% of the total variance of the observations. MAE equal to 0.92 d yr^{-1} is lower than the standard error of the estimates (1.16 d yr^{-1}), while the Kling-Gupta index is -0.18. Again, there is no significant serial autocorrelation in the residuals (DW = 2.27, $p > 0.05$). The model's predictive capability may have decreased with the generally more sporadic snowfall events occurred in recent decades, which appears to be a southern

Europe-wide process (Diodato et al. 2021). In fact, there is a mismatch from 1978 onwards in the validation period timelines showing the co-evolution of SDY between observations and estimates (Fig. 6A). However, the associated distribution of the model residuals (Fig. 6B) does not significantly differ ($p > 0.05$) from what would be expected for a normally distributed sample.

In determining whether the SDY (BNV) model can be simplified, we have fitted a multiple linear regression model between SDY and three independent inputs: $(0.25 + SSI)^{1.4}$, $(28.5 - Tw - Ts)^2$ and $VC(T(w \rightarrow s)_{t=-1}^{t=0})$ of Eq. (1). All of the variance components in the model are significant (the highest p-value being 0.0061 for the term VC) and the model cannot be simplified further.

3.2 Reconstruction of snow days per year in the Benevento Valley

Eq. (1) was used to reconstruct the evolution of SDY over the period 1645–2018 (Fig. 7A). Each year includes the winter season started on December of the previous year.

The reconstructed data were then analysed to find out possible trends and/or climatic oscillations explaining most of the observed variance in the long-term time-series of SDY, and to compare contemporary snowfall with historical snowfall. Overall, the estimated SDY values present a significant decreasing trend ($p < 0.05$) for the total period (Fig. 7A). However, this decrease was not gradual and dominated during the 20th and early 21st centuries. The wavelet power spectrum of the time-series also shows temporal inhomogeneity in the SDY (Fig. 7B), with significant periodicities detected mainly at the beginning of the study period (90% confidence interval).

Consequently, we distinctly analysed SDY during three climatic sub-periods: (i) the Maunder Minimum (MM, 1645-1715), as it marks the end of a period of rapid cooling in

1600s; (ii) the Late Little Ice Age (LLIA, 1716-1866); and (iii) the Modern Warming Period (MWP, 1867-2018). The application of test statistics suggests the existence of a change-point in 1866 (Buishand 1982) or 1910 (Pettitt 1979), which can be seen as a transition phase indicator from the LLIA to the MWP. Change detection suggests however that 1866 is a main breakpoint as it detects a structural change owing to the exit from the LLIA (~1850).

Table 1 shows that the mean and median values of SDY (modelled series) undergo a jump between MM and LLIA (6.0 and 4.7 versus 4.5 and 3.6 d yr^{-1}) and between LLIA and MWP (4.5 and 3.6 versus 3.3 and 2.8 d yr^{-1}). For the three time-slices, a higher mean than median indicates that in each sub-period few years have much higher SDY values than most of the rest. The percentage of years with snow days above the 95^{th} and 98^{th} percentiles (9.8 and 11.3 d yr^{-1}, respectively) is also markedly different in the three sub-periods considered, with a greater difference between the first and the following two sub-periods. In particular, the higher percentage of years exceeding the 95^{th} (14%) and the 98^{th} (7%) percentiles confirms that the Maunder Minimum corresponded to an extreme climatic phase in southern Italy, implying the occurrence of recurring highly impacting snowy events. We know from Moio and Sussana (1977) manuscript (p. 244) that winter seasons during the Maunder Minimum were often hard, and winter conditions extended over spring months: *In the year 1658, on April 18, the day of Holy Thursday, a lot of snow fell which raised a palm followed by an ice; all the vines were dried which were tender with great shortage of wine which for two years was sold at a very high price*. Similar conditions also occurred in the autumn 1680, springs 1684 and 1694, and in May 1705 (Diodato et al. 2019).

The recent trend towards warmer conditions indicates that rising temperatures are the main factor that triggered the decline of both SDY and cold spells during the 20th and early 21st century. The trend test returns a statistically significant decrease in SDY during the MWP ($p < 0.05$), whereas no trend ($p > 0.05$) is detected in the MM and the LLIA (Table 1). Observed records indicate (Fig. 7A) that the 95th percentile was exceeded four times after the change-point year: in 1935, 1940, 1956 and 1963 with 10, 13, 10 and 10 d yr^{-1}, respectively. In 1940, with 13 snow days, the 98th percentile was also exceeded. It is important to consider that whether the 95th percentile was caught in 1940, the modelled peak values are all below that value after the change-point. According to the overall tendency of the observed records, which is representative of snowfall changes in the BNV, the model estimates do not always fit the snowfall peaks. Thus, it can also be assumed that the high SDY values occurred in the past could not be fully captured in the modelled time-series.

3.3 Influence of atmospheric-oceanic circulation patterns

We analysed the links between large-scale atmospheric-oceanic circulation patterns and snowfall in different climatic sub-periods (MM, LLIA and MWP) through linear correlations between low-pass filtered standardized SDY anomalies (>11 years cut-off period) and gridded reconstructions of: (1) air surface temperature (T; Luterbacher et al. 2004); (2) mean sea-level pressure (mslp; Luterbacher et al. 2002); and (3) sea-surface temperature (SST; LMR and HadISST).

The increase of SDY at the BNV during the three sub-climatic periods is generally associated with an anomalous high-pressure system located over northern (Figs. 8A, B) or north-western (Fig. 8C) Europe and an anomalous low over the eastern Mediterranean.

These large-scale configurations (consistent with those described in Section 2.1) favour the advection of cold continental air from the east-northeast towards Southern Italy (Fazzini et al. 2005, Dafis et al. 2016), which can moisten as it crosses the Adriatic Sea in a ways analogous to lake-effect snow in the Great Lakes region (Shi & Xue 2019). As expected, colder-than-usual surface air temperatures are observed over large parts of Europe (including the BNV) for all three sub-climatic periods, associated with the SDY increase (Figs. 8A-C). Differences in the position of the anomalous high over northern European latitudes could be attributed to the modulating role of global average temperatures (minimum during the MM) for the advection of cold and moist air towards the BNV, but also to the uncertainties associated with our reconstructed time-series (larger during the MM; Luterbacher et al. 2004). Despite correlation between SDY and low-frequency (> 11-yr) NAO reconstructed time-series (Jones et al. 1997, Trouet et al. 2009, Tardif et al. 2019) returns negative values for their temporal overlapping periods, these are not statistically significant ($p > 0.05$). The fact that mslp anomalies associated with SDY appear displaced downstream in the North Atlantic (Figs. 8A-C) compared to the canonical NAO pattern (Pinto & Raible 2012) may explain this outcome.

For completeness, Fig. 8D presents the results for the MWP with linear trends removed. As expected, the cooling associated with the SDY enhancement is weaker over the European continent (with global warming signal removed) and the associated large-scale pattern appears clearer. Similar correlation results with global SSTs are provided in Figs. 8E, F (only significant patterns for climatic sub-periods shown). During the MM, the SDY enhancement appears to be related to SST anomalies in the North Pacific and North Atlantic (Fig. 8E) that resemble the positive phase of the Pacific Decadal Oscillation

(PDO). Linear correlation between SDY and the PDO index (from LMR) during the MM returns a statistically significant value (0.46, $p < 0.05$) and is consistent with the significant periodicities detected in SDY in Fig. 7B (around 20 to 60 years). However, this is not evident during the LLIA and MWP periods (not shown). We refrain at this point from proposing any causal relationship between PDO and SDY during the MM, which would require a much more detailed analysis supported by additional climate reconstruction databases (beyond the scope of this paper). For the AMO, no robust correlation was found with SDY in any of the sub-periods studied.

Finally, the SST correlation results in Fig. 8F for the MWP are also worth mentioning. As this period is clearly dominated by the impact of global warming, the figure shows a robust global anti-correlation signal with SDY. When the linear trend was removed from the time-series, no correlation pattern with SST anomalies (from both LMR and HadISST datasets) was observed (not shown).

4. DISCUSSION

According to Camuffo et al. (2010), for the Mediterranean area, a major effort to transform early observations into homogenized series through rigorous quality controls, validation and correction became possible only after the 17th century. We thus used 1645 data onwards because weather data at earlier times were reconstructed from non-instrumental proxies only and, as such, were affected by larger uncertainties (Diodato et al. 2014). Thanks to our reconstruction, we can now comment and discuss on single, exceptional winter seasons. Observing Fig. 7A, it stands out the surprising number of snowy days (32) occurred in 1683-1684 during the MM. This is the estimated absolute maximum value of the modelled time-series, which exceeds by over 10 times the standard deviation of the entire series (2.96 d yr^{-1}). The extraordinary cold winter 1683-1684 was particularly long and harsh, with unusual low mean temperatures, passed into the historical chronicles because of its bitter coldness and snowstorms (Diodato & Bellocchi 2011). We refer to the Moio and Sussana (1977) manuscript (p. 247), reporting a long period of winter weather from January to April 1684: *with heavy snowfalls and continuing frost in southern Italy, with winter that was severe almost always covered with snow and ice and so continued and large that froze rivers and perished all the citrus trees.* In the Corradi (1865-1890) annals (vol. II, p. 257), 1684 is also identified as a remarkable year, during which snow covered the ground until after Easter (occurred on April 2nd). In Fig. 9A, the January to March 1684 anomalies of reconstructed surface air temperature (Luterbacher et al. 2004) and mslp (Luterbacher et al. 2002) compared to the long-term seasonal mean are shown. Consistent with the historical chronicles, colder than usual conditions were present over the BNV and the rest of Europe, with regional departures of up to -6 ºC from the long-term seasonal mean (north-eastern Europe). The anomalous large-scale mslp conditions of that year are also consistent with the findings in Fig. 8, with positive anomalies over Scandinavia and negative over the Mediterranean, promoting the advection of cold continental air from the east into the BNV.

To find a similar atmospheric configuration throughout the winter season, one has to go to the winters of 1829-1830 and 1939-1940. In the winter of 1830 (Fig. 9B), atmospheric conditions were similar to those of 1684. The most notable difference is the location of the coldest temperature anomalies over central and eastern Europe. That winter was one of the earliest and longest of those examined in the BNV, with abundant snow from mid-November to the end of March, which was lethal for agriculture in many parts of Europe

(Corradi 1865-1890). Copious snow also fell in Rome and, in January 1830, the press was suspended due to heavy snowfall, which prevented the mails from arriving (Serbati 1974).

In the winter of 1939-1940 (Fig. 9C), the cold anomalies appear less pronounced over southern Europe and the anomalous mslp conditions differ slightly, with the anomalous high centred near Iceland (as in Figs. 8C-D) and the low west of Iberia. This configuration also favoured the advection of cold continental air from the northeast into Europe. For that winter, almost 10 days of snow were estimated in the BNV. In Naples, eight days of snow were recorded, with 35 cm depth and trains at a standstill (Majo 1958). Copious snowfall was also recorded in Rome, with 15-30 cm of snow depth (Mangianti & Beltrano 1991), while 11 days of snow were registered in Florence (Borchi & Macii 2011).

After the winter 1955-1956, which exceeded the 95th percentile with its 12 days of snowfall in February, winters never again reached that extreme value. These results are consistent with data indicating that temperature-induced precipitation has shifted from snow to rain during the MWP (Fig. 7A), with a general trend of decreasing snowfall in the central Apennines (Perugia station, Pandolfi & Lorenzetti 1996) and the Swiss alpine region (Diodato et al. 2020b). This is not surprising, as the reconstruction approach used here relies mainly on parameters related to air temperature. Although this variable is crucial for snowfall, additional factors may play a determinant role in the context of global warming (D'Errico et al. 2020), which makes future projections of snowfall still a difficult task.

5. CONCLUSIONS

This study provides insights into the long-term fluctuations of snow days per year (SDY) over a 374-year period (from 1645 to 2018) in the Benevento Valley in southern

Italy. A detailed dataset was compiled in the region based on records available from two main stations (Benevento city observatory and the Met European Research Observatory) since 1870. Then, they were reconstructed back to 1645 using a parsimonious model sensitive to winter and spring temperatures and a storm-severity index based on historical documentary sources. It is important to highlight the relevance of this unique long-term dataset for studying changes in snowfall in an area where the literature on this subject is scarce. Indeed, this variable is crucial to better understand climate-change impacts on the energy balance and the water cycle, with important implications for sectors such as agriculture and tourism.

The reconstructed SDY time-series shows a change-point in 1866, after which a significant decrease is observed. Overall, the trend of decreasing snow days since the outbreak of the LIA is in line with previous literature, not only in relatively close areas of Italy and Europe, but also elsewhere. Before the change-point year, no trends were detected during the Maunder Minimum (1645-1715) and the LLIA (1716-1866). The statistically significant link observed between SDY and the Pacific Decadal Oscillation during the Maunder Minimum, which is not sufficient to uncover the underlying physical mechanisms of this relationship given the uncertainties present in past data, is a clue for further analyses. What instead emerges in all sub-periods is that the large-scale circulation conditions fostering snowfall in the BNV were generally characterized by an anomalous high-pressure system located over northern-north-western Europe and an anomalous low over the eastern Mediterranean. These conditions favour the advection of cold continental air from the Balkan Peninsula and Siberia, which moistens as it crosses the Adriatic Sea towards the BNV.

Although the results presented in this study are specific for the BNV, our statistical modeling approach could potentially be applied to adjacent Mediterranean or additional regions where reliable long-term snowfall records were available and surface temperature advection from poleward regions (determined by atmospheric circulation patterns; Croce et al. 2018) was the dominant driver for snowfall occurrence. Nevertheless, further studies on extended spatial scales are necessary to disentangle the mechanisms behind climatic drivers and snow cover responses, especially in the context of future climate projections (D'Errico et al. 2020).

Acknowledgements

This was an investigators-driven study without financial support.

Data availability

Long-term seasonal temperature and monthly sea level pressure reconstruction datasets over Europe from Luterbacher et al. (2002, 2004) and reconstructed North Atlantic Oscillation indices from Trouet et al. (2009) and Jones et al. (1997): Climate Explorer (monthly and seasonal historical reconstructions; monthly and annual climate indices): https://climexp.knmi.nl; CRU Global Climate Dataset: Time-series of variations in climate with variations in other phenomena v3: https://catalogue.ceda.ac.uk/uuid/3f8944800cc48e1cbc29a5ee12d8542d; Last Millennium Reanalysis (LMR) Project Global Climate Reconstructions Version 2: https://www.ncdc.noaa.gov/paleo-search/study/27850; Met Office Hadley centre for the

HadSST database: https://www.metoffice.gov.uk/hadobs/hadsst4; Additional data and codes can be available upon request to the authors.

Author contribution

N. D. developed the original research design and collected and analysed the historical documentary data. N. D. and G. B. wrote the first draft of the article and made the analysis and interpretations of Figs. 1 to 7. I. G. made the analyses and interpretations of Figs. 8 and 9 and wrote the final manuscript version, which was reviewed by all authors.

Competing interests

The authors declare no competing interests.

REFERENCES

Borchi E, Macii R (2011) La neve a Firenze (1874–2010). Pagnini ed., Florence, Italy, in Italian.

Braconnot P, Vimeux F (2020) Past and future contexts for climate and water-cycle variability, and consequences for the biosphere. Past Global Changes Magazine 28(1)

Briffa KR, Jones PD, Schweingruber FH, Osborn TJ (1998) Influence of volcanic eruptions on Northern Hemisphere summer temperature over the past 600 years. Nature 393:450-455

Buishand TA (1982) Some methods for testing the homogeneity of rainfall records. Journal of Hydrology 58:11-27

Camuffo D, Bertolin C, Barriendos M, Dominguez-Castro F and others (2010) 500-year temperature reconstruction in the Mediterranean Basin by means of documentary data and instrumental observations. Climatic Change 101:169-199

Capozzi V, Montopoli M, Bracci A, Adirosi E, Baldini L, Vulpiani G, Budillon G (2020) Retrieval of snow precipitation rate from polarimetric X-band radar measurements in Southern Italy Apennine mountains. Atmospheric Research 236:104796

Clark MP, Serreze MC, Robinson DA (1999) Atmospheric controls on Eurasian snow extent. International Journal of Climatology 19:27-40

Corradi A (1865-1890) Annali delle epidemie occorse in Italia dalle prime memorie fino al 1850, 5, Reprint in 1972 by Arnaldo Forni, Bologna, Italy, in Italian.

Croce P, Formichi P, Landi F, Mercogliano P, Bucchignani E, Dosio A, Dimova S (2018) The snow load in Europe and the climate change. Climate Risk Management 20:138-154

D'Errico M, Yiou P, Nardini C, Lunkeit F, Faranda D (2020) A dynamical and thermodynamic mechanism to explain heavy snowfalls in current and future climate over Italy during cold spells. Earth Syst Dynam Discuss 2020:1-35

Dafis S, Lolis CJ, Houssos EE, Bartzokas A (2016) The atmospheric circulation characteristics favouring snowfall in an area with complex relief in Northwestern Greece. International Journal of Climatology 36:3561-3577

De Renzi S (1829) Osservazioni sulla topografia-medica del Regno di Napoli, P. II. Tipografia Fratelli Criscuolo, Naples, Italy, in Italian.

DeWalle DR, Rango A (2008) Principles of Snow Hydrology. Cambridge University Press, Cambridge, United Kingdom.

Diodato N (1997) Paesaggi d'Inverno: Aspetti naturalistici e climatologici delle nevicate sulla Campania interna. La Provincia Sannita, 17, Benevento, Italy, in Italian.

Diodato N, Bellocchi G (2011) Discovering the anomalously cold Mediterranean winters during the Maunder minimum. The Holocene 22:589-596

Diodato N, Bellocchi G, Bertolin C, Camuffo D (2014) Climate variability analysis of winter temperatures in the central Mediterranean since 1500 AD. Theoretical and Applied Climatology 116:203-210

Diodato N, Büntgen U, Bellocchi G (2019) Mediterranean winter snowfall variability over the past millennium. International Journal of Climatology 39:384-394

Diodato N, Bellocchi G (2020) Climate control on snowfall days in peninsular Italy. Theoretical and Applied Climatology 140:951-961

Diodato N, Bertolin C, Bellocchi G (2020a) Multi-Decadal Variability in the Snow-Cover Reconstruction at Parma Observatory (Northern Italy, 1681–2018 CE). Frontiers in Earth Science 8

Diodato N, Fratianni S, Bellocchi G (2020b) Reconstruction of snow days based on monthly climate indicators in the Swiss pre-alpine region. Regional Environmental Change 20:55

Diodato N, Bertolin C, Bellocchi G, de Ferri L, Fantini P (2021) New insights into the world's longest series of monthly snowfall (Parma, Northern Italy, 1777–2018). International Journal of Climatology 41:E1270-E1286

Doretti N (1950) L'Osservatorio Meteorologico di Benevento nel suo ottantennio, 23, in Italian.

Enzi S, Bertolin C, Diodato N (2014) Snowfall time-series reconstruction in Italy over the last 300 years. The Holocene 24:346-356

Fazzini M, Giuffrida A, Frustaci G (2005) Snowfall analysis over peninsular Italy in relationship to the different types of synoptic circulation: First results. Croatian Meteorological Journal 40:650-653

Godsey SE, Kirchner JW, Tague CL (2014) Effects of changes in winter snowpacks on summer low flows: case studies in the Sierra Nevada, California, USA. Hydrological Processes 28:5048-5064

Grundstein A, Mote TL (2010) Trends in Average Snow Depth Across the Western United States. Physical Geography 31:172-185

Hammer O, Harper D, Ryan P (2001) PAST: Paleontological Statistics Software Package for Education and Data Analysis. Palaeontologia Electronica 4:1-9

Henderson GR, Peings Y, Furtado JC, Kushner PJ (2018) Snow–atmosphere coupling in the Northern Hemisphere. Nature Climate Change 8:954-963

Jennings KS, Winchell TS, Livneh B, Molotch NP (2018) Spatial variation of the rain–snow temperature threshold across the Northern Hemisphere. Nature Communications 9:1148

Jones PD, Jonsson T, Wheeler D (1997) Extension to the North Atlantic oscillation using early instrumental pressure observations from Gibraltar and south-west Iceland. International Journal of Climatology 17:1433-1450

Jones PD, Harris IC (2008) Climatic Research Unit (CRU): Time-series (TS) datasets of variations in climate with variations in other phenomena v3. NCAS British Atmospheric Data Centre

Kling H, Fuchs M, Paulin M (2012) Runoff conditions in the upper Danube basin under an ensemble of climate change scenarios. Journal of Hydrology 424-425:264-277

Knight JR, Folland CK, Scaife AA (2006) Climate impacts of the Atlantic Multidecadal Oscillation. Geophysical Research Letters 33

Lean J, Beer J, Bradley R (1995) Reconstruction of solar irradiance since 1610: Implications for climate change. Geophysical Research Letters 22:3195-3198

Luterbacher J, Xoplaki E, Dietrich D, Rickli R and others (2002) Reconstruction of sea level pressure fields over the Eastern North Atlantic and Europe back to 1500. Climate Dynamics 18:545-561

Luterbacher J, Dietrich D, Xoplaki E, Grosjean M, Wanner H (2004) European Seasonal and Annual Temperature Variability, Trends, and Extremes Since 1500. Science 303:1499

Majo A (1958) Le nevicate a Napoli (1866-1957). Bollettino della Società dei Naturalisti in Napoli, 67, 1-11, in Italian.

Mangianti F, Beltrano MC (1991) La neve a Roma dal 1741 al 1990. Italian Ministry of Agriculture and Forestry - Central Bureau of Agricultural Ecology, Rome, Italy, in Italian.

Mantua NJ, Hare SR (2002) The Pacific Decadal Oscillation. Journal of Oceanography 58:35-44

Martínez-Ibarra E, Serrano-Montes JL, Arias-García J (2019) Reconstruction and analysis of 1900– 2017 snowfall events on the southeast coast of Spain. Climate Research 78:41-50

Mercalli L, Di Napoli G (2008) Il clima di Torino. Società Meteorologica Subalpina, Moncalieri, Italy, in Italian.

Miller GH, Geirsdóttir Á, Zhong Y, Larsen DJ and others (2012) Abrupt onset of the Little Ice Age triggered by volcanism and sustained by sea-ice/ocean feedbacks. Geophysical Research Letters 39

Moio GB, Sussana G (1977) Diario di quanto successe in Catanzaro dal 1710 al 1769. Effe Emme Ed., Chiaravalle, Italy, in Italian.

Mulligan M, Wainwright J (2013) Modelling and Model Building. John Wiley and Sons Ltd., Chichester, United Kingdom.

Navarro-Serrano FM, López-Moreno JI (2017) Spatio-temporal analysis of snowfall events in the spanish Pyrenees and their relationship to atmospheric circulation. 2017 43:22

Pandolfi AM, Lorenzetti MC (1996) Due secoli di nevicate a Perugia: Analisi preliminare. Nimbus 4:55-57

Pettitt AN (1979) A Non-Parametric Approach to the Change-Point Problem. Journal of the Royal Statistical Society Series C (Applied Statistics) 28:126-135

Pinto JG, Raible CC (2012) Past and recent changes in the North Atlantic oscillation. WIREs Climate Change 3:79-90

Rayner NA, Parker DE, Horton EB, Folland CK and others (2003) Global analyses of sea surface temperature, sea ice, and night marine air temperature since the late nineteenth century. Journal of Geophysical Research: Atmospheres 108

Serbati R (1974) Studi sul pensiero filosofico e religioso dei secoli XIX e XX. Marzorati Editore, Milan, Italy, in Italian.

Shi Q, Xue P (2019) Impact of Lake Surface Temperature Variations on Lake Effect Snow Over the Great Lakes Region. Journal of Geophysical Research: Atmospheres 124:12553-12567

Stuiver M, Braziunas TF (1993) Sun, ocean, climate and atmospheric 14CO2 : an evaluation of causal and spectral relationships. The Holocene 3:289-305

Tardif R, Hakim GJ, Perkins WA, Horlick KA and others (2019) Last Millennium Reanalysis with an expanded proxy database and seasonal proxy modeling. Clim Past 15:1251-1273

Trouet V, Esper J, Graham NE, Baker A, Scourse JD, Frank DC (2009) Persistent Positive North Atlantic Oscillation Mode Dominated the Medieval Climate Anomaly. Science 324:78

Wang S, Zhou F, Russell HAJ (2017) Estimating Snow Mass and Peak River Flows for the Mackenzie River Basin Using GRACE Satellite Observations. Remote Sensing 9:256

Webster M, Gerland S, Holland M, Hunke E and others (2018) Snow in the changing sea-ice systems. Nature Climate Change 8:946-953

WMO (2009) Handbook on climate and climate temp reporting. World Meteorological Organisation, Geneva, Switzerland.

Xie H, Li D, Xiong L (2014) Exploring the ability of the Pettitt method for detecting change point by Monte Carlo simulation. Stochastic Environmental Research and Risk Assessment 28:1643-1655

Yarnell SM, Viers JH, Mount JF (2010) Ecology and Management of the Spring Snowmelt Recession. BioScience 60:114-127

Table 1: Descriptive statistics of the modelled SDY time-series for three climatic sub-periods (MM: Maunder Minimum; LLIA: Late Little Ice Age; MWP: Modern Warming Period). Trends detected through Mann-Kendall test ($p < 0.05$).

Climatic sub-period (CE years)	**Central tendencies**		**Percentiles**		**Trend**
	Mean (standard deviation)	**Median**	**>95th**	**>98th**	
	d yr^{-1}		**% of years**		**d 10^{-2} yr^{-1}**
MM (1645-1715)	6.0 (4.9)	4.7	14.0	7.0	No
LLIA (1716-1866)	4.5 (2.6)	3.6	5.9	2.0	No
MWP (1867-2018)	3.3 (1.9)	2.8	<1.0	0.0	-1.1

Fig. 1: The slopes of Mount Vesuvius under the snow, seen from Torre del Greco (40° 47′ N, 14° 22′ E) in an image of an anonymous of the 19th century (http://www.vesuvioweb.com/it/2012/01/raffaele-de-maio-un-altro-vesuvio).

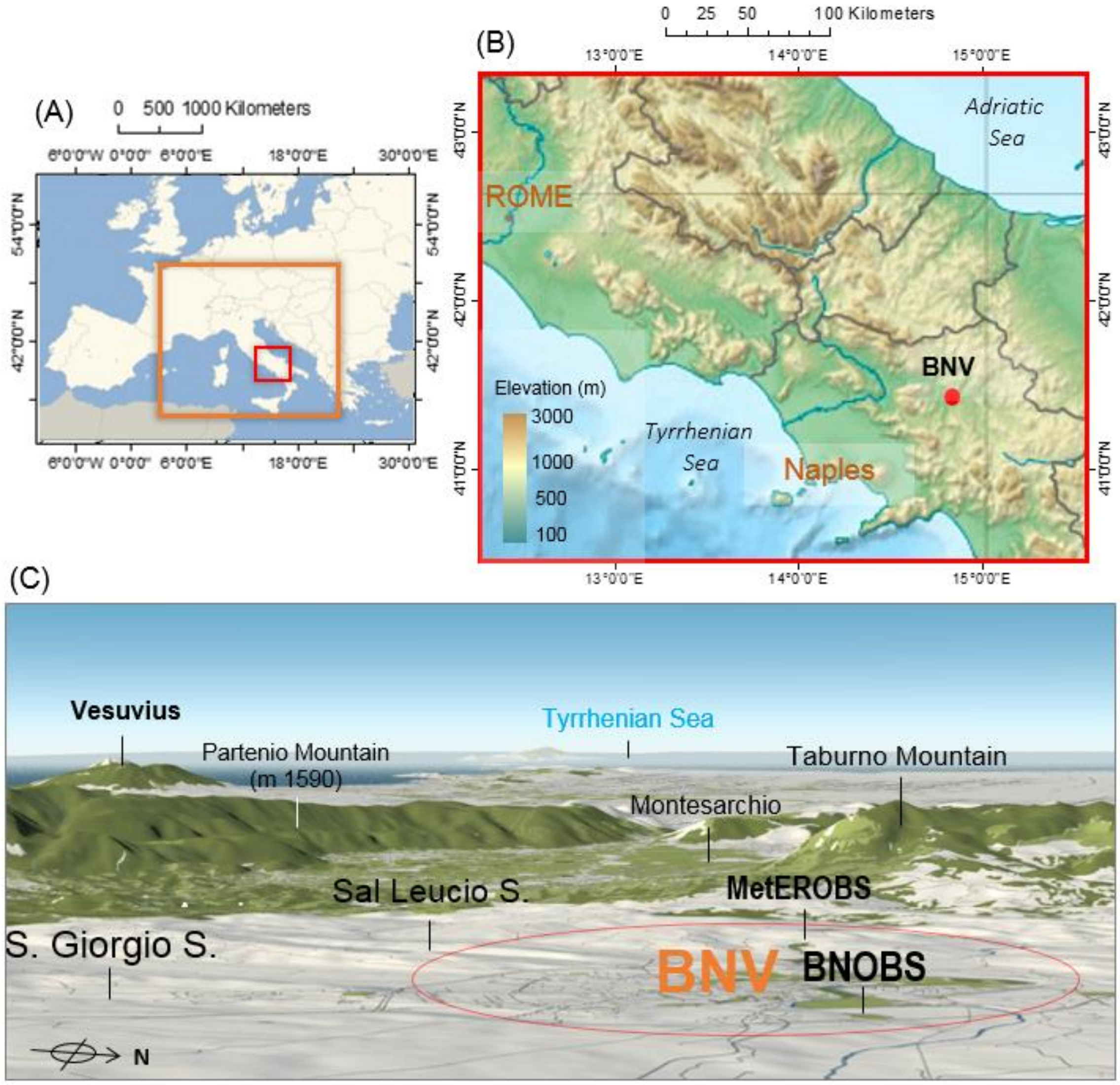

Fig. 2: (A) Geographical setting in Europe, with central-southern Italy. (B) location of the Benevento Valley (BNV) and terrain elevation (colours in m a.s.l.). (C) Perspective view of the Benevento Valley (BNV) between the Partenio and Taburno mountains and the east Apennines (not visible). Maps are authors' own elaboration from free, public domain images: (A) ESRI (http://www.esri.com) archive; (B) Wikipedia (https://it.wikipedia.org/wiki/Italia#/media/File:Italy_topographic_map-blank.svg); and (C) OpenStreetMap (https://demo.f4map.com/#camera.theta=0.9).

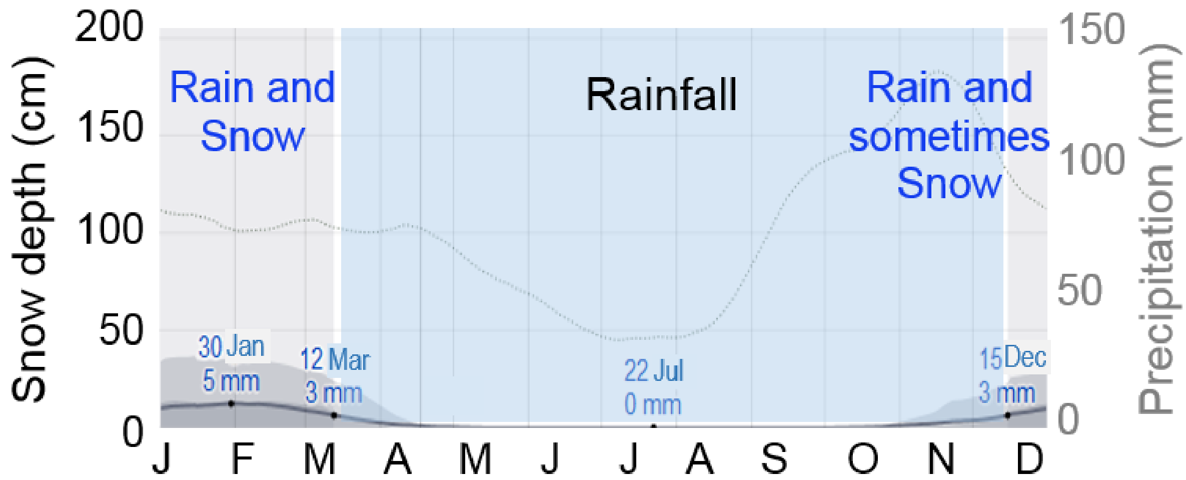

Fig. 3: Monthly mean distribution of snow depth (thick black line) and seasonal precipitation regime (coloured vertical bands and grey dotted curve) at the Benevento Valley (BNV), with the 90th percentile of snow depth (light grey line and area beneath), calculated over the period 1971-2018. Output generated from data freely available in Weather Spark archives (goo.gl/VEPQwt).

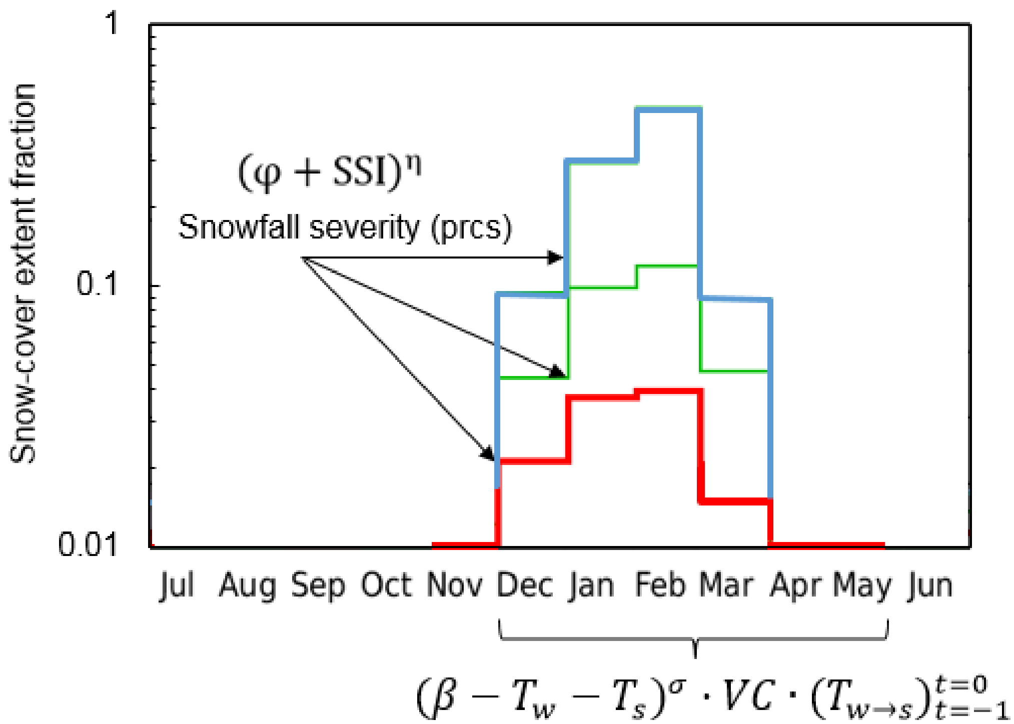

Fig. 4: Monthly snow-cover extent fraction in Italy (50th percentiles in red, 80th percentiles in green, 98th percentiles in blue), with the associated driving factors. Percentiles (prcs) were calculated on data provided for the period 1966-2018 by Global Snow Lab - Rutgers University Climate Lab (https://climate.rutgers.edu/snowcover) via KNMI-Climate Explorer Climate Change Atlas (http://climexp.knmi.nl). The two main terms of Eq. (1) are reported.

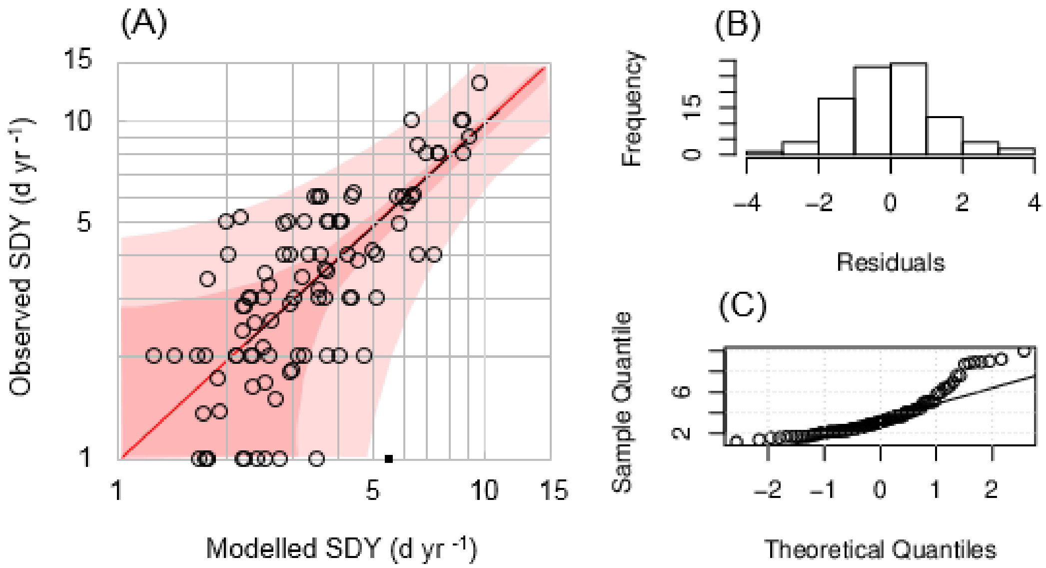

Fig. 5: (A) Scatterplot of observed and modelled SDY for the calibration sub-set (1870-1968 CE), with regression line (red line), the inner bounds showing 99% confidence limits (pink coloured band), and the outer bounds showing 90% prediction limits for new observations (light pink coloured area); axes are in log-scale; (B) histogram of residuals; (C) Q-Q plot (sample versus theoretical quantile values).

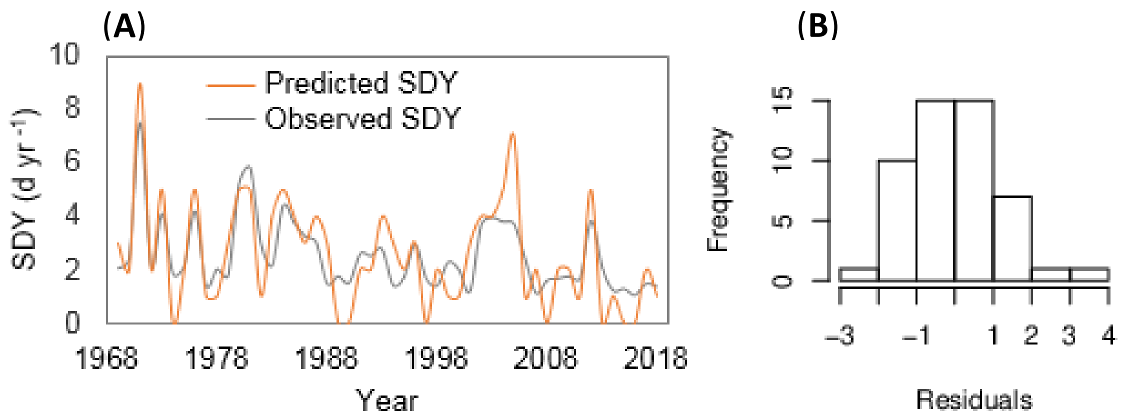

Fig. 6: (A) Timeline co-evolution of observed and modelled SDY (see legend) for the validation period (1969-2018 CE); (B) histogram of residuals.

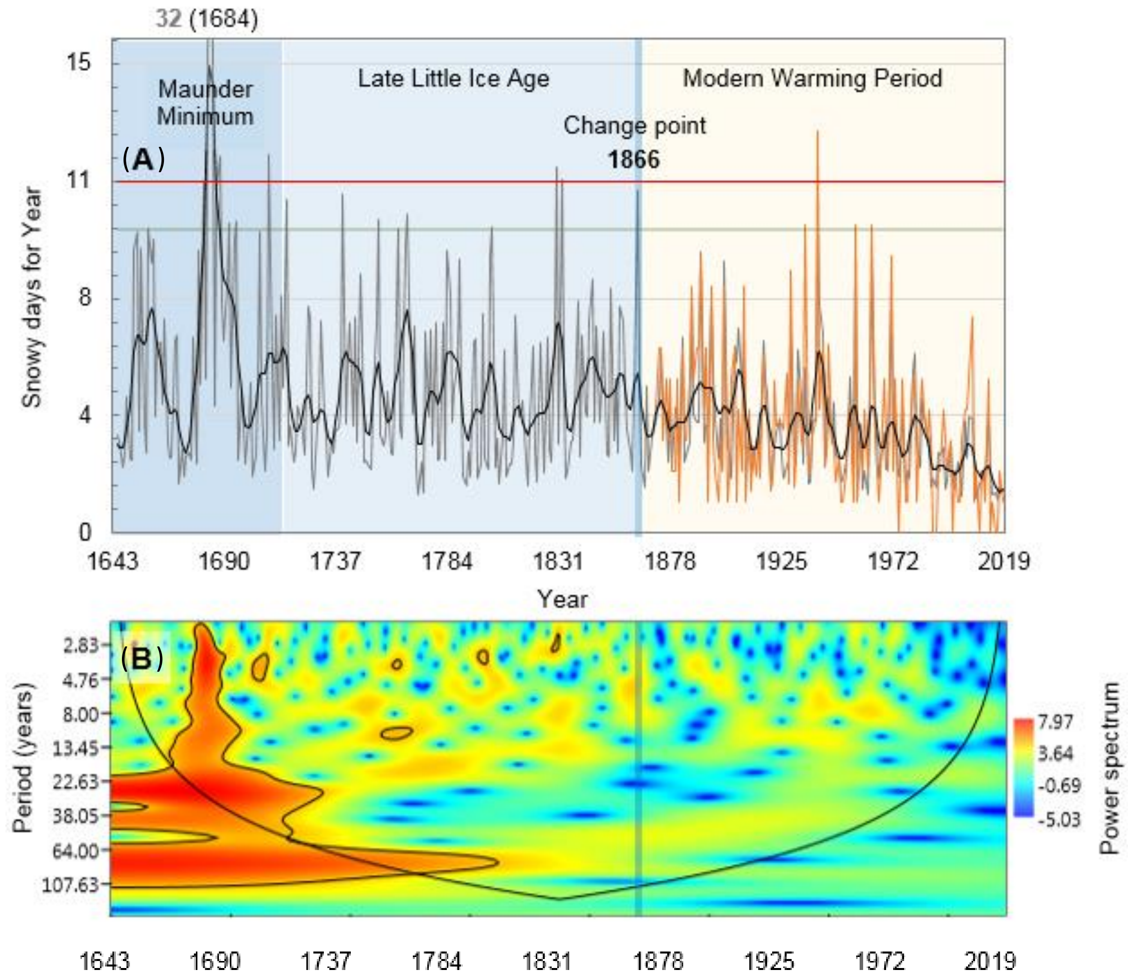

Fig. 7: (A) Snow days per year (SDY) at Benevento Valley in the period 1645-2018 CE. Timeline of modelled SDY data (grey curve) with a 11-year Gaussian Filter (black curve), and overimposed observed records for the period 1870-2018 CE (orange curve); grey and red horizontal lines are the 95th and 98th percentile, respectively, while blue vertical line indicates the change-point year (1866). (B) Wavelet power spectrum with Morlet basis function for the reconstructed SDY time-series; bounded colours identify p-values < 0.1; the bell-shaped, black contour marks the limit between the reliable region and the region above the contour where the edge effects occur (arranged from Hammer et al. 2001).

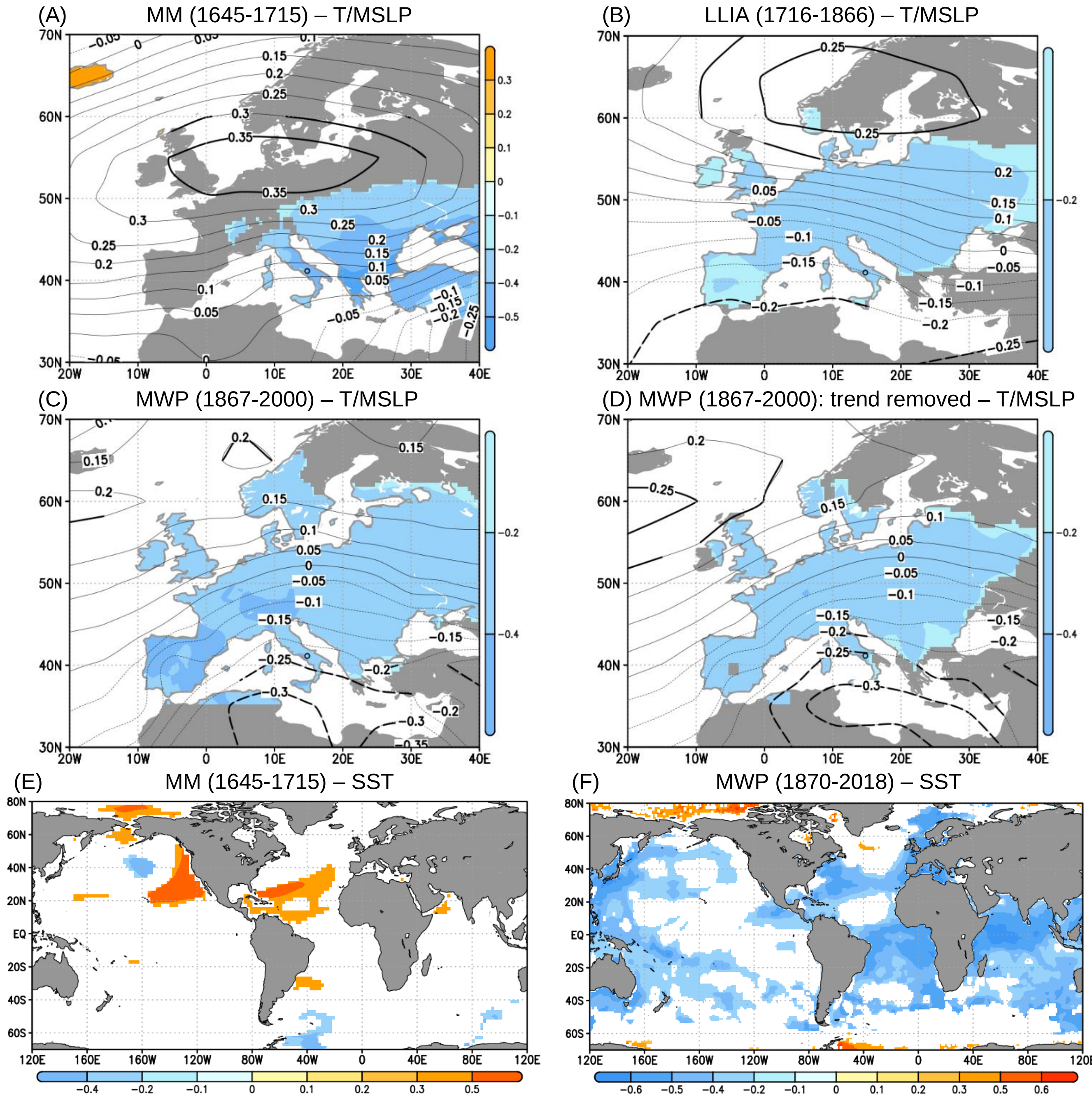

Fig. 8: (A) Correlation between standardized low-pass filtered (>11-yr) SDY anomalies at the BNV and gridded surface air temperature (Luterbacher et al. 2004) in ºC (shadings at 95% confidence interval) and mean sea-level pressure (Luterbacher et al. 2002) in hPa (contours, 95% confidence interval in thick lines) anomalies for the period January-March 1645-1715 (MM). BNV location marked with open circle. (B-C) Same as (A) but for 1716-1866 (LLIA) and 1867-2000 (MWP). (D) Same as (C) but with linear trend removed. (E) Same as (A) but for correlation with sea-surface temperature (SST; from Last Millenium Reanalysis) in ºC (shadings at 95% confidence interval) annual anomalies for the period 1645-1715 (MM). (F) Same as (E) but for the period 1870-2018 (MWP) from HadISST.

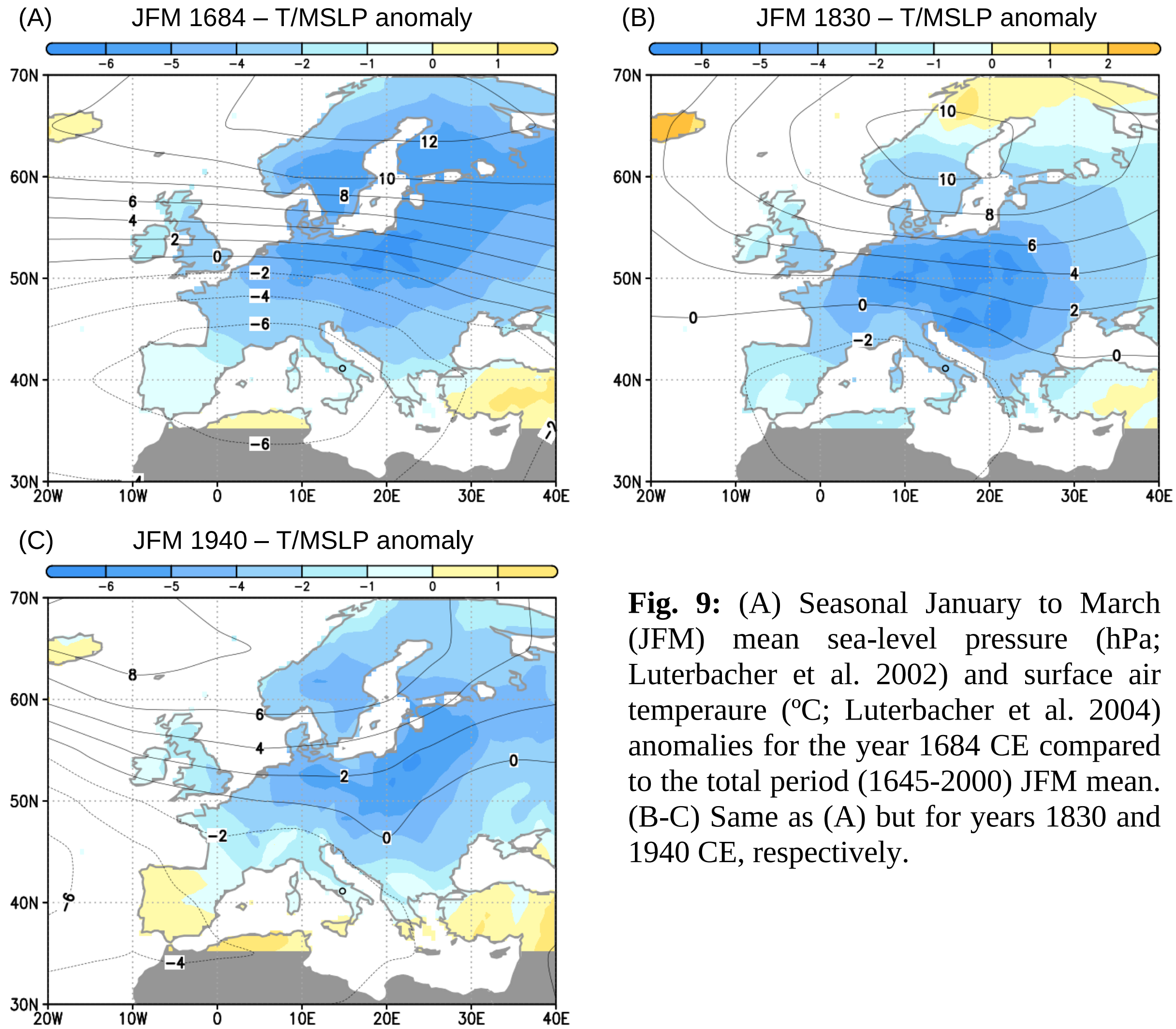

Fig. 9: (A) Seasonal January to March (JFM) mean sea-level pressure (hPa; Luterbacher et al. 2002) and surface air temperaure (ºC; Luterbacher et al. 2004) anomalies for the year 1684 CE compared to the total period (1645-2000) JFM mean. (B-C) Same as (A) but for years 1830 and 1940 CE, respectively.